Chemical Physics 21 (1977) 373–383

EXCITON PERCOLATION. II: NAPHTHALENE $^1B_{2u}$ SUPERTRANSFER *

R. KOPELMAN, E.M. MONBERG and F.W. OCHS ‡
Department of Chemistry, The University of Michigan, Ann Arbor, Michigan 48109, USA

Received 10 November 1976

The exciton percolation theory has been tested for the migration of the lowest singlet exciton in our model organic alloy system at low temperature (2 K): binary isotopic mixed crystals of naphthalene ($C_{10}H_8$–$C_{10}D_8$), with an added exciton sensor (supertrap) of betamethylnaphthalene (about 10^{-3} mole fraction). At these relatively high sensor concentrations the system's migration dynamics are described quantitatively by the simple limiting case of *supertransfer*, i.e. by a *dynamic percolation formulation* of Hoshen and Kopelman *that depends only on the concentrations and interaction topology* of the ternary crystal. Experimentally, the exciton's migration dynamics is monitored by fluorescence spectra, taken under controlled conditions (crystal quality, purity, concentration, excitation and temperature). The effects of exciton tunneling (superexchange), exciton–phonon coupling, coherence, exciton delocalization and non-equilibrium chemical solubility are considered. We show that a complete concentration study of this simple energy transport model system reveals four kinds of exciton transfer regions, but only one (above the critical guest site percolation concentration) with long ranged, multistep, direct guest exciton transport. The same study, on the low concentration side, yields relative trapping efficiencies and thus eliminates the need for adjustable parameters. The substitutional randomness of the isotopic mixed crystal is confirmed, as well as the short range nature of the $^1B_{2u}$ exciton interactions and the dominance of the interchange equivalent, nearest neighbor, pairwise (molecular) excitation ($^1B_{2u}$) exchange integrals in the pure, perfect, low-temperature, naphthalene crystal. Our present exciton percolation study is also relevant to the primary energy transport process in heterogeneous photosynthetic units.

1. Introduction

The problem of electronic energy transfer in mixed molecular crystals can be handled by a combination of exciton [1–5] and percolation theory [5–7]. Exciton theory helps to explain the translational and interchange equivalent interactions [5], the importance of deep and shallow trap states in isotopic and chemically mixed crystals [1–3, 5], and the extent of coherence in the excitonic motion [4]. Tunneling by the excitons through potential barriers [1, 5] and the temperature dependence of the exciton's behaviour [4] are also relevant here. These problems have attracted much attention and a considerable level of success has been attained in their solution. Here we report the application of the above mentioned exciton concepts, along with recent exciton percolation theory [8] (part I of series), to the interpretation of the fluorescence spectra of isotopic and chemical mixed single crystals of naphthalene.

The percolation problem has been tackled by the computer simulation of large binary lattices, as an analytical solution to the problem is unavailable at this time [6]. We make use of the now available *distribution*, i.e. *frequency of occurrence*, of resonance guest *clusters* in *binary lattices* [9]. These, in turn, depend only on the topology of the lattice and the concentration of the quest species [10, 11]. A detailed theoretical treatment of site–bond percolation and the accompanying computer program [12] are also utilized here. The appropriate topology for the site percolation problem in the naphthalene system is determined by the relative strengths of the neighboring exciton pairwise interactions [5].

Naphthalene crystallizes in an orthorhombic lattice

* Supported by NSF Grant DMR75-07832 A01 and NIH Grant NS08116-08.
‡ Present address: Cal-Farm Insurance Co., Berkeley, California 94705, USA.

with 2 molecules per primitive unit cell [13]. It has been shown for the lowest singlet exciton that the strongest interaction ($\approx 18\ cm^{-1}$) occurs along the $\pm\frac{1}{2}(a \pm b)$ direction, i.e. between the nearest-neighbor interchange equivalent sites [14–17]. If, in the first approximation, we neglect the weaker interactions of the next-nearest-neighbors (i.e. the out-of-the-a b-plane interactions), the locus of these $\pm\frac{1}{2}(a \pm b)$ molecular centers describes a two-dimensional lattice with each site having four nearest neighbors. Thus the topology is equivalent to a square lattice. We vary the concentration of the guest–host system, $C_{10}H_8$ in a $C_{10}D_8$ host lattice, to determine the effect of cluster distribution (i.e. cluster frequency) on the singlet fluorescence, by a modified sensitized emission approach. Wolf and Port [18] have studied this binary system for guest concentrations up to 0.50. In comparison, our system includes a third component, a constant ($\approx 10^{-3}$) fraction of betamethylnaphthalene (BMN), the notorious impurity [19], providing a deep trap, relative to either $C_{10}H_8$ or $C_{10}D_8$. We call the BMN the *supertrap* in order to distinguish it from the *trap* species, naphthalene ($C_{10}H_8$). The supertrap acts as a sensor for measuring the *multistep* exciton transfer through the lattice. As the concentration of the guest is increased we observe an abrupt exciton insulator-to-conductor transition by monitoring the increase in the relative emission of the supertrap. By definition, the guest system includes both traps and supertraps, but it contains mostly traps ($C_{10}H_8$). Our method, in contrast to others [18], is designed to follow the longer range exciton transport in the guest quasilattice, and to distinguish it from the shorter range, trap-to-trap tunneling of the singlet exciton.

The *host* is, by definition, the species with the highest excitation energy to the first singlet state. When the sample is irradiated by a broad band UV source the initial distribution of excitation is, to the first approximation, proportional to the concentration of each constituent. The host $C_{10}D_8$ transfers its excitation very rapidly to either a nearby trap or supertrap site. Since for both Δ (trap-depths to $C_{10}H_8$ or BMN), $\Delta \gg kT$ (at 1.7 K), the transfer is essentially irreversible with respect to phonon assisted thermalization back into the host band. Those supertraps that are initially excited contribute a constant low level of BMN emission, somewhat analogous to a "dark current" (being present even when the exciton flow is "off"). As mentioned, a guest exciton can either arise from direct guest excitation or from host excitation followed by transfer to guest.

If we neglect cluster-to-cluster tunneling at this stage we can assume that a guest exciton is then trapped in a guest cluster of size m, where m can be any integer, from a monomer up to an "infinite" cluster [8]. The question now is whether the guest exciton, trapped in a cluster of size m, will find a supertrap, within its lifetime, and thus emit from the BMN first singlet level. Excitons trapped in smaller guest clusters, not containing a supertrap, will eventually fluoresce from the lowest $C_{10}H_8$ cluster level to the ground state. We can get an estimate of the total number of site-to-site jumps an exciton can make if we use the relationship [20, 21] $T_j \approx (4M)^{-1}$, where T_j is the jump-time and M is the absolute pairwise interaction in hertz. For naphthalene $^1B_{2u}$ we get, for $M \approx 18\ cm^{-1}$, $T_j \approx 5 \times 10^{-13}$ s. Using [11, 20] an exciton lifetime τ of about 100 ns, one gets the total number of "steps"; $\tau/T_j \approx 2 \times 10^5$ jumps. One would assume, with these many jumps, that if the cluster size m approaches $(C_S)^{-1}$, where C_S is the supertrap concentration, i.e. when the cluster is likely to contain at least one supertrap, that there should be an excellent chance for the exciton to visit a supertrap site within its lifetime. The latter is always true, by definition, in the supertransfer [8] limit.

The set of parameters which will place the exciton's behaviour in a cluster within the domain of supertransfer calls for a combination of long exciton lifetime and/or large exciton pairwise interaction and/or efficient trapping [7, 22–25]. We show here that the naphthalene first singlet system, for supertrap concentrations above 5×10^{-4}, falls within this realm of exciton supertransfer. The supertrapping efficiency is shown to be above 0.1. A brief report of this has appeared earlier [25].

2. Synopsis of theory

It has been shown [8] that, in the limit of supertransfer, the probability for *any* guest exciton to be trapped by the supertrap, for a given topology and guest concentration, is:

$$P = \bar{P}_\infty [1-(1-\bar{P}_\infty)^Z] + \sum_{m \neq m'} [1-(1-m/G)^Z] i_m m/G . \qquad (1)$$

Here $\bar{P}_\infty$ is the probability that a guest molecule belongs to an "infinite" cluster, m' is the index of the "infinite" cluster (maxicluster), Z is the effective [8] number of supertrap sites, G is the total number of guest sites and i_m is the occurrence frequency of clusters of size m. This equation is valid [8] only in the limit of supertransfer and where $1 \ll Z \ll G$. For guest concentrations C_g just below the critical site percolation concentration C_g^c, several "large" clusters will emerge, just before they coalesce into the "infinite" cluster. For these clusters severe fluctuations arise in the computations [7, 12]. The summation over the entire cluster distribution, for a finite lattice, can be performed by the computer and the quantity P thus evaluated as a function of C_g for different topologies. We note that the quantities $\bar{P}_\infty$ and i_m only require a *binary* lattice computer simulation. At concentrations outside the critical percolation region C_g^c, eq. (1) can be simplified [8, 11], giving $P = Z/G$ at $C_g \to 0$ and $P = \bar{P}_\infty$ at $C_g \to 1$.

A mechanism of trap-to-trap migration via superexchange tunneling through intervening host sites is used to explain both the results from our low guest concentration singlet experiment and the triplet studies on the same system [22]. We can think of this resonance interaction as occurring between two isolated guest clusters in a host matrix. An exciton localized on one cluster can be pictured as tunneling through a potential barrier to another guest cluster. The higher and wider the potential barrier, the weaker is the interaction. In this case, the height of the potential barrier is Δ, the trap depth from the bottom of the pure host band to the center of the guest band (monomer), and the width is determined by the number of host sites separating isolated guest clusters. The time necessary to tunnel from trap to trap through this potential wall is given by [21, 22]

$$t_{(0,n)} = \Delta^{n-1}/4\Gamma_n \beta^n c\,. \tag{2}$$

Here $n-1$ is the number of intervening host sites, β is the pairwise interaction energy (in cm^{-1}), c is the speed of light and Γ_n is a geometrical factor, given by the number of paths, involving n bonds, between the two trap sites [21]. An expression which relates this tunneling time to the time necessary for an exciton to have an even chance of finding a supertrap is [21]

$$t = \Delta^{\bar{n}-1}/4\bar{C}_S \gamma \bar{\Gamma}_{\bar{n}} \beta^{\bar{n}} c \lesssim \tau_g\,, \tag{3}$$

where τ_g is the guest exciton lifetime, $\bar{C}_S$ is the concentration of the supertrap relative to the guest, $\bar{n}$ is the effective maximum range of interaction, $\bar{\Gamma}_{\bar{n}}$ is the *average* geometrical factor for paths of length $\bar{n}$ and γ is the trapping efficiency. If the time necessary for the exciton to find a supertrap is longer than the singlet lifetime, then the tunneling mechanism is effectively blocked. The temperature dependence of the singlet exciton has also been studied in these systems and will be presented elsewhere [23]. Exciton coherence and the non-supertransfer regime [7] are discussed elsewhere [24].

3. Experimental

Variable amounts (0.01 to 0.99 mole fraction) of protonated naphthalene $C_{10}H_8$ (James Hinton, Newport, Va.), which had been previously potassium-fused, and zone-refined for 150 passes, were doped into 99 atom%-deuterium perdeuteronaphthalene, $C_{10}D_8$ (Thompson–Packard) along with a relatively constant amount ($\approx$ 1%) betamethylnaphthalene. Single crystals were grown from the melt via a modified Bridgman technique and were annealed to relieve internal chain. Cleaved crystals less than 1 mm thick were mounted strain-free and immersed in supercooled liquid helium at 1.7 K. The crystals were excited with 2400–2900 Å radiation by an appropriately filtered [17, 25] Hanovia 1600 W xenon lamp. The fluorescence was monitored at right angles to the excitation by a 1 meter Jarrell–Ash double grating spectrometer with 0.5 cm^{-1} resolution in second order. The signal was measured [26] using an SSR digital photon counter with simultaneous calibration from an iron hollow cathode lamp (using a PAR chopper). Data were processed using computer programs described earlier [17, 26].

The concentration of the trap ($C_{10}H_8$) component in these mixed crystals was determined by mass spectrometry. The BMN concentration cannot be obtained in this manner and UV absorption was utilized for the more dilute (in BMN) samples. These UV measurements gave only relative values since the molar extinction coefficient for BMN in naphthalene at 1.7 K is not known (but see discussion below). The best analytical method found was that of high resolution gas–liquid chromatography. A 10′ DEGS capillary column was used with a flame ionization detector. Several samples were taken

Table 1
Concentration of trap, supertrap and I_S/I_{total}

$C_{10}H_8$ (%)	BMN (%)	$I_S/(I_S + I_t)$ (%)	$I_S/(I_S + 1.9I_t)$ (%)
1.2	0.04	6.4	3.5
4.8	0.03	12.3	6.9
5.6	0.09	4.4	2.4
8.3	0.02	3.9	2.1
9.9	0.09	9.7	5.3
17.1	0.05	2.6	1.4
30	0.02	1.9	1.0
35	0.02	4.8	2.6
44.2	0.07	29.4	18
51.4	0.18	72.9	58
58.1	0.09	62.2	46
64.9	0.20	91.1	85
74.5	0.04	94.1	89
83.5	0.69	> 99	> 99
94.5	0.16	> 99	> 99
99.9	0.08	>99	> 99

from each crystal and dissolved in hexane with an average concentration value resulting for each crystal. Thus the BMN concentrations listed in table 1 actually are weighted averages of the chromatographic and absorbance determinations. The mixed crystal reproducibility is discussed in the appendix.

4. Results and discussion

The emission from the supertrap was monitored by observing the intensity of the betamethylnaphthalene 0–0 band at about 31065 cm^{-1}. There is no discernible frequency shift for this band as the *guest* concentration is increased. The trap emission is followed via the intense naphthalene 510 cm^{-1} vibronic band. We have previously dealt with the strong concentration dependence of this band's frequency [27]. Fig. 1 shows the spectral region of interest for eight different guest concentrations. The absolute intensities have all been normalized for illustrative purposes.

The relative intensities of the $C_{10}H_8$ and BMN bands and their change with guest concentration is of primary importance for our interpretation of the dynamic percolation in these mixed crystals. The integrated intensities were obtained with the aid of a CRT graphics terminal and a spectral analysis program described elsewhere [26]. The major problem in the calculation of these integrated intensities is that, for most guest concentrations, the intense naphthalene amalgamated phonon sidebands built upon the BMN origin tend to obscure both the naphthalene vibronic band and its corresponding phonon sidebands. The *total* intensity originating from *either* the trap or the supertrap is the sum of the principal band intensity plus *its* phonon sidebands.

An additional complication arises because of the differential coupling strength of the naphthalene delocalized phonons to excitons of $C_{10}H_8$ and BMN

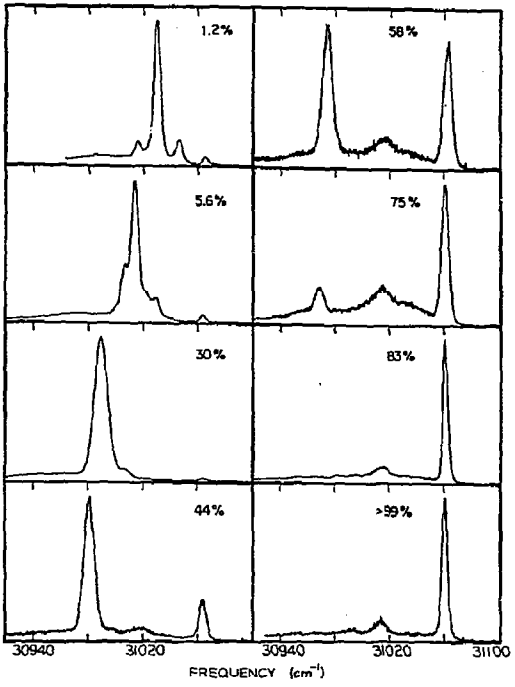

Fig. 1. Trap and supertrap fluorescence spectra of the ternary system: $C_{10}H_8$–$C_{10}D_8$–BMN. The concentration of BMN is held constant at about 10^{-3} mole fraction (table 1). The mole percent values refer to the $C_{10}H_8$ concentration. The most striking observation is that as the $C_{10}H_8$ concentration increases, the $C_{10}H_8$ (vibronic, 510 cm^{-1}) fluorescence (30 970–31 030 cm^{-1}) *decreases drastically*, with the BMN emission (0–0 band at 31065 cm^{-1}) increasing proportionately. The band at about 31 015 is a phonon sideband built upon the BMN origin. The spectra were obtained at 2 K, on a 1 meter double grating Jarrell–Ash spectrometer with 20 μ slits (≈ 2 cm^{-1} resolution), with xenon lamp excitation (and appropriate filters) and recorded via computer interfaced photon counting, with calibration and processing methods described elsewhere [26]. BMN is β-methylnaphthalene. The absolute photon count scales [26] are normalized for ease of illustration.

[24, 28, 29]. The monomer BMN exciton, with a narrower bandwidth than that of the naphthalene resonance clusters, is more strongly coupled to the phonons than is the latter. Thus it was necessary to obtain a ratio of the principal band intensity to its corresponding phonon sidebands for both the trap and the supertrap. The spectra of the 30% $C_{10}H_8$ in $C_{10}D_8$ shows, for reasons which will be explained later, the minimum amount of BMN emission relative to $C_{10}H_8$ emission, thus minimizing the BMN phonons interference in the guest emission region. For the ratio $C_{10}H_8$ 0–510 phonon sidebands/$C_{10}H_8$ 0–510 principal band, a value of 0.17 was found. The intensities of the phonon bands were integrated out to about 100 cm^{-1} from the principal band. These integration limits include [32] over 95% of the total one-phonon band.

The corresponding ratio for the supertrap, BMN 0–0 phonon sidebands/BMN 0–0 origin band = 1.14, was obtained from the 99% $C_{10}H_8$ spectra, where all the emission emanates from the supertrap. Assuming that these ratios are independent of C_g, it is straightforward to measure the intensity of both the BMN origin and the $C_{10}H_8$ 0–510 cm^{-1} vibronic band, multiplying each by the appropriate phonon sideband correction factor and comparing the total relative intensities. Table 1 shows the results of the integrations for the whole range of guest and supertrap concentrations, including the following considerations. The integrated spectral intensities do not directly reflect the ability of an exciton to find a sensor. The difference in radiative yields [21] for the BMN 0–0 origin and the $C_{10}H_8$ vibronic (510 cm^{-1}) origin has to be considered, along with the relative trapping efficiency for the trap and supertrap. The probability of a singlet exciton finding a sensor, normalized to equal radiative yield and trapping efficiency, can be expressed as

$$P = \frac{I_S/K_S\gamma_S}{I_S/K_S\gamma_S + I_t/K_t\gamma_t}; \tag{4}$$

rearranging we get

$$P = \frac{I_S}{I_S + I_t(K_S\gamma_S/K_t\gamma_t)} \equiv \frac{I_S}{I_{total}}, \tag{5}$$

where I_S and I_t are the integrated spectral intensities of the BMN and $C_{10}H_8$ fluorescence in fig. 1, γ is a trapping efficiency and K is a radiative yield (or efficiency). The naphthalene vibronic (510 cm^{-1}) absorbance is about a factor of 1.9 ± 0.2 weaker than the 0–0 BMN one. This is based on old but apparently reliable work [30], using organic glass matrices at 77 K. We assume this ratio (F_S/F_t) to be roughly correct for our integrated fig. 1 transitions at 2 K in our mixed crystal systems, i.e. ignoring changes in Franck–Condon factors (F) from absorption to fluorescence as well as changes in medium and temperature. However, we note that these corrections are either small or tend towards mutual cancellation, as can be seen from the following consideration. It may be helpful to reflect at this stage that, in the limit of no trap-to-supertrap energy transfer, one has (neglecting direct absorption):

$$I_t/I_S = C_t\gamma_t K_t/C_S\gamma_S K_S \approx C_t\gamma_t\tau_t F_t/C_S\gamma_S\tau_S F_S. \tag{6}$$

From the 1.2% sample (table 1) we can find the relative (trapping and radiative) efficiency, since at this low guest concentration there is little trap-to-trap or trap-to-supertrap migration of excitons, as will be explained later. Knowing the relative concentration ratio $\bar{C}_S$ (table 1), and the integrated spectral intensity ratio $I_S/(I_S + I_t) = 0.064$, we find that the relative trapping and radiative efficiency $K_S\gamma_S/K_t\gamma_t$ is equal to about the oscillator strength ratio of 1.9. Thus we can calculate the value of P from eq. (5), see table 2. We note that the trapping efficiencies might vary with guest concentration, but we had to neglect this variation. On the other hand, the variation of the radiative yield (per molecule) with concentration is believed to be negligible [5]. It should be noted that the influence of both γ and K on P is largest for small values of P (i.e. $I_t \gg I_S$) and smallest for $P \to 1$ (i.e. $I_t \ll I_S$). In addition, the following affects the results of table 1. At low guest concentration, the trap–host transition (0–496) has to be included in the integrated host emission. This transition arises because of the slight delocalization of the trap electronic excitation (Rashba effect [3]) and has recently been quantitatively determined in our laboratory [31]. This correction is most important at low guest concentrations (≈ 1%), as can also be seen in fig. 1, and has been fully taken into account in this work. Note that as $C_g \to 0$ both eqs. (1) and (5) give $P \to \bar{C}_S$ ($\equiv C_S/C_g = \bar{Z}/G \equiv$ "dark current").

In fig. 2 we see the experimental data points compared with the curves derived from the percolation theory discussed earlier [8, 9], see eq. (1). At this point we discuss the uncertainties in the values of I_S/I_{total}.

Table 2
Mole percent concentrations of molecules, for trap, supertrap and trap clusters in samples of interest

Total $C_{10}H_8$	Total BMN	$C_{10}H_8$ monomer	$C_{10}H_8$ dimer	$C_{10}H_8$ trimer [a]	$C_{10}H_8$ tetramer [a]
1.2	0.04	1.14	0.06	b) –	–
4.8	0.03	3.94	0.68	0.14	0.03
5.6	0.09	4.44	0.88	0.21	0.05
8.3	0.02	5.88	1.64	0.55	0.17
9.9	0.09	6.52	2.10	0.81	0.30
15.0 [c]	–	7.83	3.40	1.85	0.95
17.1	0.05	8.06	3.78	2.26	1.28
20.0 [c]	0	8.19	4.20	2.82	1.79
25.0 [c]	0	7.91	4.50	3.44	2.52
27.5 [c]	0	7.60	4.40	3.58	2.77
30	0.02	7.20	4.23	3.60	2.91
35	0.02	6.24	3.69	3.33	2.88
44.2	0.07	4.28	2.35	2.23	2.02
51.4	0.18	2.88	1.40	1.29	1.17
58.1	0.09	1.79	0.73	0.65	0.55
64.9	0.20	0.99	0.31	0.24	0.20
74.5	0.04	0.31	0.06	0.03	0.02
83.5	0.69	0.06	–	–	–
94.5	0.16	–	–	–	–
99.9	0.08	–	–	–	–

a) See ref. [43].
b) A dash designates a lower than 0.01% concentration.
c) Calculated values.

There are three primary contributions to the error bars shown in fig. 2. The first is the one discussed above, concerning relative molar trapping and radiative efficiencies of trap and supertrap. The second involves the integration methods used for determining the relative emission intensities. The frequency limits of integration for each peak were set with some degree of arbitrariness, since the spectra were not deconvoluted. Included in this category is the fact that, at best, the calculated phonon contribution factor is good to only ± 10%. The magnitude of this error is at a maximum in the concentration range of $C_g = 0.55 \pm 0.15$, for it is here that there is the maximum overlap of the BMN phonon sidebands with the $C_{10}H_8$ vibronic (510 cm^{-1}) band. The third, and most intriguing contribution arises from the variation in the actual (versus nominal) BMN concentration.

The effect of a varying supertrap concentration upon supertrap emission is strongly dependent on the guest concentration. As the concentration of the guest increases so does the average size of guest clusters. The

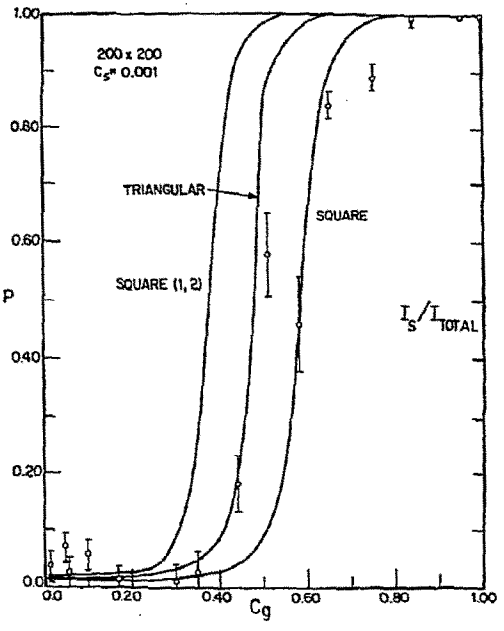

Fig. 2. Experimental and theoretical dynamical exciton percolation: first *singlet* excitation of naphthalene. The experimental points are integrated fluorescence intensity ratios I_S/I_{total} where I_S is the sensor (betamethylnaphthalene) emission intensity and $I_{total} = I_S + 1.9I_t$, the combined sensor and exciton conductor (naphthalene-h_8) emission intensity [normalized, see eq. (5)]. Here $C_S \approx 10^{-3}$ (mole fraction) so that $C_g \approx C_t$. The theoretical curves give the dynamical percolation P according to eq. (1) (4×10^4 sites) [9] for the three topologies: *square* (4 nearest, equivalent, neighbors), *triangular* (6 nearest, equivalent, neighbors) and *square (1, 2)* (8 nearest and next-nearest neighbors, all treated equivalently). Note that all three theoretical curves were calculated with the parameter $C_S = 0.001$. They would have passed through the lowest guest concentration point ($C_g \approx C_t = 0.012$, table 1) had they been calculated for its supertrap concentration ($C_S = 0.00044$, table 1). To avoid crowding, we did not draw the "dark current" line, $0.001C_g^{-1}$, for $0.1 > C_g \geq 0.001$.

region most sensitive to supertrap concentration, is that just below the percolation concentration, i.e. where there exist many large, but not "infinite", guest clusters of size comparable to $(C_S)^{-1}$. This phenomenon will be discussed in more detail elsewhere [9] but for the purposes of this paper it will suffice to show the results of a computer simulation of this problem for a two-dimensional square lattice [8,9].

Fig. 3 shows the simulation derived [9] probability P_Y of a guest site being in a guest cluster containing a supertrap. If we assume that an exciton, localized in a

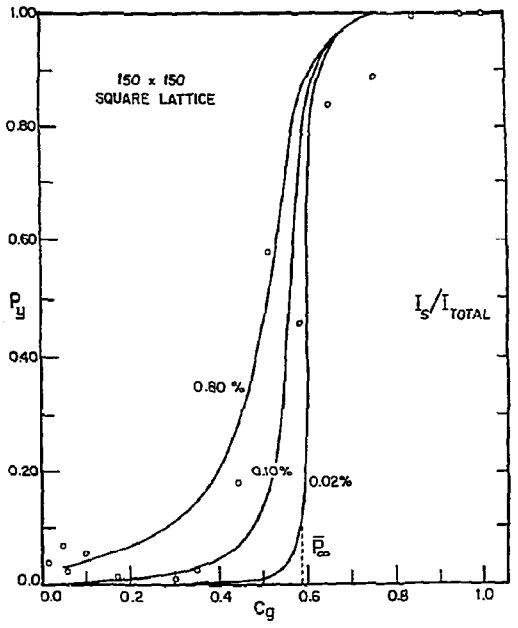

Fig. 3. A computer simulation of the exciton supertransfer versus guest concentration C_g (mole fraction) with sensor concentration C_S (mole percent) as a parameter. The 150 X 150 square lattice is generated by the computer, with the help of a random number generation subroutine, as a *ternary* system, including C_S mole percent of supertrap (sensor). P_Y is the fraction of total guest which is connected via a succession of nearest neighbor guest interactions to a sensor. $P_Y + \bar{C}_S$ is equivalent to P [eq. (1)] of fig. 2. Note the limiting $\bar{P}_\infty$ curve* (dashed) [9]. The experimental points are the same as in fig. 2. The error bars have been removed, as here each C_g point should be considered in conjunction with its specific C_S value (table 1) [40].

supertrap-containing cluster, eventually finds the supertrap, then this P_Y is equivalent to the probability P [eq. (1)] that an exciton localized on any given lattice site at time t_0 will eventually be trapped by a supertrap at a later time t, in the limit of supertransfer. We can see that, in the regions of low and high C_g, a variation in the supertrap concentration barely affects the BMN emission. Only in the region of C_g about 0.40 to 0.60 is this a crucial parameter. However, since the dynamic exciton percolation curve rises so steeply in this region, small fluctuations in the supertrap concentration will not change the general shape or position of the curve, even though the value of I_S/I_{total} changes dramatically [33]. If we further reduce the supertrap concentration, as shown in fig. 3, we obtain a curve almost identical to that for $\bar{P}_\infty$, as now only the "infinite" cluster would have a non-zero probability [34] of including a scarce supertrap. However, as C_S is lowered in this manner, the assumption of supertransfer may no longer be valid and some of the excitons in the "infinite" cluster may be converted to trap emission before they ever find a supertrap. In this domain of low C_S, factors such as exciton jump time, coherence lengths, lifetime perturbations and a trapping efficiencies become very important. The effects of these physical factors are discussed elsewhere [7, 11, 24, 40].

Our experimental points in fig. 3 do fit the theoretical curve for a square lattice with considerable success [40]. Since in this theoretical treatment next nearest interactions were not considered (as a first approximation), we expect the actual experimental dynamic percolation to occur at a lower guest concentration than would be predicted for a square lattice topology. Upon consideration of the four most important exciton interactions [16, 17], an interaction topology which is a *weighted* average, with respect to the pairwise interaction energies of square, triangular, square (1, 2) and cubic topologies [7, 11, 20], should match the experimental points even more closely (compare the unweighted curves of fig. 2). This is discussed further below.

5. Direct transfer, tunneling and the range of exciton transport

The range of *naphthalene guest concentrations* $C_t (= C_g - C_S \approx C_g)$ can be divided into four fairly distinct regions for the purpose of explaining the ratio of I_S/I_{total}. The *first* region is that of $C_t < 0.015$. This region is dominated by excitons trapped on monomers and small guest clusters. For very low concentrations of guest, $C_g \to 0$, all we expect from eq. (1) is the "dark current" ($P = \bar{C}_S$) and, indeed, the normalized "relative" fluorescence of BMN and monomeric naphthalene, I_S/I_{total}, is equal (by normalization, see above) to their "relative" concentration, $C_S/C_g = \bar{C}_S$. At $C_t = 0.01$, the effective separation (in the $a\,b$ plane) between guest sites is more than 10 intervening host molecules [9, 21]. The trap-to-trap direct (dipole–dipole [2]) transfer time is about 10–100 ns and the tunneling time about the same [35], while the excitons' lifetime [36] is about 100 ns; so there is little or no trap-to-trap migration [37]. Thus in *region 1* there is *little*

guest exciton transfer, rather it is dominated by trapping from the host exciton bond ("dark current").

In *region 2*, $0.05 \leqslant C_t \leqslant 0.40$, important changes occur. The first is that the relative concentration of supertrap to guest, $\bar{C}_S$ is decreasing steadily. Thus the proportion of supertrap emission, due to direct absorption decreases. Concomitantly, the supertrap's chance of host trapping is steadily decreasing as well, because the number of guest traps (monomers, dimers, trimers, etc.) is increasing (see table 2). Hanson [14], Hong and Robinson [38], Wolf [18] and work in this laboratory [10, 11, 16, 22, 24, 27] have shown that the larger clusters have energy states lower than that of the monomers. At low kT, these shallow resonance-guest-cluster traps compete very effectively with the supertraps for the guest monomer excitons, as these clusters are more abundant than the supertraps (see table 2). This competition mainly involves tunneling. Actually, *region 2* is characterized by *guest exciton transfer via tunneling*, with some direct dipole–dipole transfer.

In the above region ($0.05 \leqslant C_t \leqslant 0.4$) the average separation between isolated guest clusters becomes less and less as C_t increases. The tunneling mechanism begins to become very important in the singlet exciton for C_t as low as 5–10%. Thus the monomer fluorescence band disappears completely at about 20%, despite a high concentration of monomers still remaining in the crystal (table 2), simply because trap-to-trap migration via tunneling allows the $C_{10}H_8$ exciton to be trapped by $C_{10}H_8$ clusters larger than monomers. Simultaneously, the cluster emission increases while the relative supertrap emission decreases (see fig. 2).

One might expect that as the $C_{10}H_8$ monomers become more abundant, and therefore in closer proximity to each other, the corresponding monomer–monomer tunneling (or dipole–dipole interactions) would lead to eventual trapping by the isolated BMN. For an even chance of being trapped by a BMN sensor, the exciton would only have to make $1/\bar{C}_S$ jumps. However, when the concentration of monomers is high enough (around 5%) [39] for efficient tunneling, the concentration of the dimer resonance clusters (see table 2) exceeds that of the supertrap by more than one order of magnitude.

As the monomer–monomer tunneling becomes more efficient, the concentration ratio of clusters (dimer + trimer + ...) to BMN increases, until at about 20% guest, where the monomer concentration is at a maximum of 0.082, the combined concentration of these larger clusters is more than 100 times the BMN concentration. The dimer concentration, which reaches a maximum value of 0.045 at 25% C_t, barely reaches the concentration necessary for efficient dimer–dimer tunneling, and even then the ratio of (trimer + tetramer + ...)/BMN is about 20.

In the case of trimers, their concentration never exceeds 0.03, thus there will be little trimer–trimer tunneling since the trimer clusters are too far apart from each other. Thus for the monomer, where site-to-site tunneling does occur, and for the dimer, where site-to-site tunneling barely occurs, only around $C_t = 0.30$, the exciton is almost always trapped by the more abundant dimer or trimer, respectively, rather than by the BMN.

Since the monomer–dimer and dimer–trimer energy separation is greater than kT, at 1.7 K, the exciton has a very poor chance of returning, via thermalization plus transfer, to a monomer site, once it is trapped by a dimer. The probability of returning to a monomer or dimer is equally poor for an exciton trapped by a trimer or larger cluster. Thus in *both* low C_t domains we expect to see little emission from the supertrap. This is borne out by fig. 2, where we see the 30% $C_{10}H_8$ sample having the lowest proportion of BMN emission of all the samples.

In *region 3*, $0.4 < C_t < 0.5$, the larger guest clusters have a high probability of containing at least one supertrap and so the emission from the latter increases. As C_g ($\approx C_t$) increases, more and more of the excitons find their way into the larger clusters and consequently are trapped out by BMN. *Region 3* is thus characterized by *multistep direct guest exciton transfer over relatively short distances* (see below).

Above the critical site percolation concentration we enter *region 4* where the amount of supertrap emission is closely approximated by the function $\bar{P}_\infty$ (fig. 3). Around $C_g \approx 0.80$, $\bar{P}_\infty$ becomes very close to unity and indeed we see that practically all of the emission in our samples originates from the supertrap. This remains true up to $C_g \to 1$ (figs. 2 and 3 and ref. [25]). The guest quasilattice consists mainly of the "infinite" cluster (maxicluster) [6–12] and, indeed, *region 4* is characterized by *multistep direct guest exciton transfer over relatively long distances* (see below).

Summarizing, in the low guest concentration domain, where C_g is about 1% or less, the trap and the supertrap

mainly compete for host excitons in proportion to their concentration, exciton transport being limited to the host. In the second domain, for C_g roughly between 5% and 40%, guest exciton transport happens, but mostly via tunneling (super-exchange), involving only a few exciton transfer steps, and typically only resulting in $C_{10}H_8$ (cluster) trapping. In the third domain, guest–guest direct exchange exciton transfer occurs mainly within the guest clusters, while guest cluster-to-cluster transfer still involves tunneling. The larger the cluster, the more important becomes the direct transfer and the better the probability for supertrap emission. However, the multistep guest transfer due to direct exchange is still limited to very short distances ($\ll 10^3$ Å). Only in the fourth domain, starting at about the critical guest site percolation concentration, does multistep direct exciton transport occur over relatively long distances ($\gtrsim 10^3$ Å) [24], resulting in a high probability of reaching a supertrap.

The supertrap thus acts as a register for the guest exciton *long-range transport* (migration). Also, our exciton percolation formulation, as used here, deals only with the mainly long-range (distances $\gtrsim 10^3$ Å) multiple step exciton transport (which itself is based only on the direct-exchange, short-range steps). Thus our theory and our experiment are geared towards the same phenomena. Experiments geared towards measuring superexchange (tunneling) based, *long-range steps* of exciton transfer, and the appropriate "long-range-percolation" formulation, are described elsewhere [21, 23].

Finally, we note that we utilize the low guest concentration domain, $C_g \to 0$ (keeping $\bar{C}_S \equiv Z/G \ll 1$), where eqs. (1) and (5) simply express a "dark current"-like [7] exciton transport restricted to the host quasilattice, ($P = \bar{C}_S$) and where no tunneling occurs, to derive the relative trapping efficiency γ_S/γ_t. This ratio is needed to demonstrate the character of the exciton percolation in the high guest concentration domain, $C_g^C \leqslant C_g \leqslant 1$, that is, the efficient, direct, multistep, long-range exciton transport in the guest quasilattice, at and above the critical guest percolation concentration.

6. Nearest- and next-nearest-neighbor interactions

In the present case of the first singlet naphthalene excitation [5, 17], the nearest-neighbor interactions (18 cm^{-1}) are two to three times larger than the next-nearest-neighbor interactions. To fully understand the role of next-nearest neighbor interactions one has to consider the cluster energy states. The mere definition of cluster states, like distinct dimer and trimer states, implies that long-range interactions are neglected. Otherwise the given dimer and trimer would form a guest "pentamer". However, such a "pentamer" has pseudo-localized states in its dimer part and pseudo-localized states in its trimer part, with localization times that are long compared to the excitation lifetime. We see that the definition of a cluster or cluster state becomes a matter of time, the lifetime of the cluster state versus the time-scale of the experiment. Along with the finite lifetime of the state comes a typical linewidth of the energy state. These questions have been discussed in great detail before [10, 16].

Let us call the energy difference between the lowest energy state of two clusters δ. If $\delta \gg kT$, energy transfer will be a one-way avenue, giving the region 2 behavior ($0.05 < C_g < 0.4$), where the energy cascades down the cluster energy ladder, until caught in the deepest cluster state available, within the exciton lifetime (this deepest state acting as a supertrap). We see from table 2 that, at 35% guest concentration, still nearly half the guest molecules are contained in the four smallest miniclusters (monomers to tetramers), where indeed [43] $\delta > 3\ cm^{-1} > kT \approx 1\ cm^{-1}$. Thus, as long as $\delta \gg kT$, we do not expect any significant exciton percolation (migration), even if the next-nearest-neighbor interactions M' define a topology with $C_c^S < 0.35$ (and also $M' \geqslant \delta$, see below). Obviously, at a higher temperature ($kT \geqslant \delta$) [23], exciton percolation would be possible (if $M' \geqslant \delta$, see below).

We have seen that the condition $\delta \leqslant kT$ is necessary for exciton migration among clusters where δ is an effective (average) energy separation. Another condition is that the M' interactions connecting such clusters be large enough. While a typical jump-time for $M' > \delta$ is $(4cM'\gamma)^{-1}$, where M' is in cm^{-1}, a typical jump time for $\delta \gg M'$ is $(4cM'\gamma)^{-1}(\delta/M')$, i.e., an order of magnitude longer for $\delta \approx 10\,M'$. Our cluster distribution calculations [9] show that with a square lattice (nearest-neighbor) topology one gets a majority of the guest molecules included in "midiclusters" (size 10 or larger), at guest concentrations above 40%, but below C_c^S. We also have $\delta < 1\ cm^{-1}$ for these midiclusters, i.e., $\delta < kT$. Thus we expect any $M' > 1\ cm^{-1}$ to con-

tribute significantly to energy migration at $C_g > 0.4$. However, detailed calculations [24] show that one does not reach the limit of supertransfer, for our present C_g, with any $M' < M_{12}$, i.e., supertransfer is reached only at about $C_g > 0.59$. The same conclusion is reached *qualitatively* by comparing our experimental points with the theoretical supertransfer curves for the various topologies in fig. 2. We note that the *trigonal* and *square (1, 2)* topology curves in fig. 2 are given mainly for illustration. The most important next-nearest-neighbor interaction may well be [16] an out-of-plane one ($M' = 6$ to $9\ cm^{-1}$) [17], giving (together with the nearest-neighbor interaction) a *simple cubic* topology *in the supertransfer limit.* However, the theoretical percolation curve for a simple cubic topology [7, 9, 20] in the supertransfer limit, is even further (to the "left", i.e., lower C_g side) from the experimental curve (fig. 2) than that of the *square (1, 2)* topology. Thus, in region 3 ($0.4 < C_g < 0.5$), the range of the exciton percolation (migration) is boosted by the next-nearest-neighbor interaction, even though most energy transfer steps still involve nearest-neighbor jumps.

In region 4 ($0.5 < C_g \leqslant 1.0$), the long-range exciton percolation (migration) is mainly due to nearest-neighbor interactions *above* the square lattice percolation concentration (0.59). However, in the region $0.5 < C_g < 0.6$, the *long-range* exciton migration may be significantly boosted by a few, strategically timed, next-nearest-neighbor hops. If we assume *in-plane* next-nearest interactions (i.e., along the *a* or *b* axis) [17], then fig. 2 gives the right impression, i.e., that of having a triangular topology based *quasi-supertransfer*. However, if one assumes to have out-of-plane next-nearest-neighbor interactions (i.e., along *c* or $a + c$) [17], then one may have a situation best described by a quasi-supertransfer based on a *layered* square lattice topology [9], effectively with 2 or 3 such layers (giving an effective C_g^c at about 0.50 or 0.43, respectively [9]). Previous work [7, 15–17] may bias us slightly towards the planar percolation topology [44]. The topic of exciton coherence is further discussed elsewhere [7, 11, 24].

7. Summary

Our above described naphthalene singlet exciton experiments are in excellent agreement with the *supertransfer* limit of the *exciton percolation* formulation. This agreement is achieved without any parameters, save the *assumption of a crystal interaction topology dominated by the nearest-neighbor forces*, i.e. short range exciton interactions. These interactions, however, result in multistep, long-range ($\gtrsim 1000$ Å), direct, guest exciton transport above the critical guest site percolation concentration (≈ 0.6), with shorter ranged direct guest exciton transport predominating down to about 0.4 mole fraction of guest. In the region below that, our experiments corroborate the expected cluster-to-cluster exciton superexchange transfer (tunneling). Our results are consistent with independent information on exciton–phonon interactions, exciton localization, exciton coherence and radiationless transitions in neat and mixed naphthalene crystals. The present exciton percolation model system can be thought of as a "prototype" for exciton percolation in heterogeneous molecular aggregates, including biomolecular aggregates, such as photosynthetic units (antenna) in green plants [7, 11, 20, 41, 42].

Appendix: Mixed crystal reproducibility

We note here that the preparation of isotopic mixed crystals ($C_{10}H_8/C_{10}D_8$) did not pose any unusual problems – the nominal concentrations being in excellent agreement with the analytical results (table 1). Furthermore, our spectroscopic results are consistent with our theoretical model, which is based on a random distribution of substitutional sites. A randomly substituted binary lattice is expected indeed, in view of all our previous experience [5].

On the other hand, the BMN concentration varies over more than an order of magnitude (table 1), even though we tried to prepare all samples with the same BMN concentration by mixing-in more BMN than is needed for saturation of the solid at the melting point. The reasons for this are not clear to us, but may involve supercooling of the melt before crystallization. On the other hand, no segregation occurred for any given crystal specimens over several years, at room temperature, nor during cycling between room temperature and 2 K.

We notice that there seems to be no correlation between the actual BMN concentration and the isotopic composition of the naphthalene host. Also, there is no evidence for BMN clustering. Rather, we believe that the large majority of BMN molecules occupy *substitu-*

tional sites in a *random* fashion. The above conclusion is based on the similar frequencies and lineshapes in all the BMN absorption and fluorescence spectra (i.e. fig. 1). Further corroboration of this conclusion is found in our triplet phosphorescence work, performed on the very same specimens [21].

References

[1] G.W. Robinson, Ann. Rev. Phys. Chem. 21 (1970) 429.
[2] M.R. Philpott, Advan. Chem. Phys. 23 (1973) 227.
[3] V.L. Broude and E.I. Rashba, Pure Appl. Chem. 37 (1974) 21.
[4] R. Silbey, Ann. Rev. Phys. Chem. 27 (1976) 203.
[5] R. Kopelman, in: Excited states, Vol. 2, ed. E.C. Lim (Academic Press, New York, 1975).
[6] S. Kirkpatrick, Rev. Mod. Phys. 45 (1973) 574.
[7] R. Kopelman, in: Topics in applied physics, Vol. 15. Radiationless processes in molecules and condensed phases, ed. F.K. Fong (Springer, Berlin, 1976).
[8] J. Hoshen and R. Kopelman, J. Chem. Phys. 65 (1976) 2817.
[9] J. Hoshen, E.M. Monberg and R. Kopelman, J. Stat. Phys., to be published.
[10] H.-K. Hong and R. Kopelman, J. Chem. Phys. 55 (1971) 5380.
[11] R. Kopelman, J. Phys. Chem. 80 (1976) 2191.
[12] J. Hoshen and R. Kopelman, Phys. Rev. B 14 (1976) 3438.
[13] A.I. Kitaigorodskii, Organic chemical crystallography (Consultants Bureau, New York, 1961).
[14] D.M. Hanson, J. Chem. Phys. 52 (1970) 3409.
[15] H.-K. Hong and R. Kopelman, Phys. Rev. Letters 25 (1970) 1030.
[16] H.-K. Hong and R. Kopelman, J. Chem. Phys. 55 (1971) 724.
[17] F.W. Ochs and R. Kopelman, J. Chem. Phys. 66 (1977) 1599.
[18] H.C. Wolf and H. Port, in: Proceedings of 12th European Congress on Molecular Spectroscopy Strassbourg, France, 1975, eds. M. Grosmann, S.G. Elkomoss and J. Ringeissen (Elsevier, Amsterdam, 1976).
[19] V.A. Pröpstl and H.C. Wolf, Z. Naturforsch. 18a (1963) 724, 822.
[20] R. Kopelman, J. Luminescence 12/13 (1976) 775.
[21] F.W. Ochs, E.M. Monberg and R. Kopelman, Chem. Phys. 19 (1977) 413.
[22] F.W. Ochs, Ph.D. Thesis, The University of Michigan (1974).
[23] E.M. Monberg and R. Kopelman, unpublished.
[24] P. Argyrakis and R. Kopelman, J. Chem. Phys., to be published.
[25] R. Kopelman, E.M. Monberg, F.W. Ochs and P.N. Prasad, Phys. Rev. Letters 34 (1975) 1506.
[26] F.W. Ochs and R. Kopelman, Appl. Spectry. 30 (1976) 306.
[27] P. Argyrakis, E.M. Monberg and R. Kopelman, Chem. Phys. Letters 36 (1975) 349.
[28] R. Kopelman, F.W. Ochs and P.N. Prasad, J. Chem. Phys. 57 (1972) 5409.
[29] F.W. Ochs, P.N. Prasad and R. Kopelman, Chem. Phys. Letters 29 (1974) 290.
[30] H.M. McConnell and D.D. Tunnicliff, J. Chem. Phys. 23 (1955) 927.
[31] F.W. Ochs, P.N. Prasad and R. Kopelman, Chem. Phys. 6 (1974) 253.
[32] R. Kopelman, F.W. Ochs and P.N. Prasad, Phys. Stat. Sol. 54 (1972) K37.
[33] Note that in preliminary publications [7, 11, 20, 25] I_S/I_{total} was defined slightly differently, i.e. $I_{total} \equiv I_S + I_t$.
[34] Note that in a preliminary publication [25] we used a differently normalized percolation probability, i.e. $P_\infty = C_g \bar{P}_\infty$.
[35] Based on eq. (2). See also ref. [21].
[36] M. Köhler, D. Schmid and H.C. Wolf, J. Luminescence 14 (1976) 41.
[37] The "amplification factor" of the BMN emission due to residual guest-to-guest transfer is expected to be 1--2, about the same as we find (from fig. 1) for the dimer trap emission.
[38] H.-K. Hong and G.W. Robinson, J. Chem. Phys. 54 (1971) 1369;
H.-K. Hong and R. Kopelman, J. Chem. Phys. 55 (1971) 724, 5380.
[39] Based on table 2 and eq. (3).
[40] We note here that our $C_g = 0.75$ experimental point (figs. 2 and 3) deviates significantly from any appropriate theoretical curve. It happens to be the only high guest concentration point (above C_g^C) with a very low supertrap concentration ($C_S = 0.0004$, see table 1); certainly significantly below 0.0010. Actually, discounting the trivial $C_g = 1$ point, all other points above percolation ($C_g^C \simeq 0.59$) have at least a four times higher C_S. Our calculations [7, 24] show that this sample ($C_g = 0.75$, $C_S = 0.0004$) should indeed have an I_S/I_{total} well below the supertransfer-limit based P (eq. (1) and fig. 2) or P_Y (simulation, fig. 3), independently of the [7, 24] coherence time parameter. Moreover, the experimental value is accounted for best with a coherence time value of about 10 ps. This is equivalent to an incoherence induced linebroadening of about 1 cm^{-1}.
[41] R.S. Knox, in: Photosynthesis, Vol. 2. Primary processes, ed. J. Barber (Elsevier, Amsterdam), to be published.
[42] C.E. Swenberg, R. Dominijanni and N.E. Geacintov, Photochem. Photobiol. 24 (1976) 601.
[43] J. Hoshen and R. Kopelman, Phys. Stat. Sol. B, to be published.
[44] We notice that the superexchange corrections [16] should be *scaled* by the concentration. Thus at $C_g = 0.5$, the "set 1" parameters of ref. [16] give $M = 16.5$ cm^{-1}, M' (planar) = -6 cm^{-1} and M' (out-of-plane) = 5 cm^{-1}.